2007

Analytical Expression for the Impedance Response of an Insertion Electrode Cell

Godfrey Sikha
University of South Carolina - Columbia

Ralph E. White
University of South Carolina - Columbia, white@cec.sc.edu

Publication Info

Published in *Journal of the Electrochemical Society*, Volume 154, Issue 1, 2007, pages A43-A54.

Sikha, G. & White, R.E. (2007). Analytical Expression for the Impedance Response of an Insertion Electrode Cell. *Journal of the Electrochemical Society*, *154*(1): A43-A54.
Publisher's Version: http://dx.doi.org/10.1149/1.2372695

0013-4651/2006/154(1)/A43/12/$20.00 © The Electrochemical Society

Analytical Expression for the Impedance Response of an Insertion Electrode Cell

Godfrey Sikha* **and Ralph E. White**,z**

Department of Chemical Engineering, University of South Carolina, Columbia, South Carolina 29208, USA

An analytical expression for the impedance response of an insertion cathode/separator/foil anode cell sandwich is presented. The analytical expression includes the impedance contributions from interfacial kinetics, double-layer adsorption, and solution-phase and solid-phase diffusion processes. The validity of the analytical solution is ascertained by comparison with the numerical solution obtained for a $LiCoO_2$/polypropylene/lithium metal cell. The flexibility of the analytical solution is utilized to analyze various limiting conditions. An expression to estimate solid-phase diffusion coefficient of insertion species in a porous electrode influenced by the solution-phase diffusion process is also derived.
 [DOI: 10.1149/1.2372695]

Manuscript received March 17, 2006; revised manuscript received August 8, 2006. Available electronically November 30, 2006.

Electrochemical impedance spectroscopy (EIS) technique has been extensively used in the analysis of lithium battery systems, especially to determine kinetic and transport parameters,[1-3] understand reaction mechanisms,[4] and to study degradation effects.[5-7] However, the mathematical interpretation of the impedance response of electrochemical systems is complicated by the processes occurring in the system. This drives researchers to adopt lumped circuit models[8-10] or finite transmission line models[11] to interpret impedance data. However, these types of models provide little information on the fundamental physical processes occurring in the cell. To gain more understanding of the physical processes, macrohomogenous models for porous electrodes have been used by some researchers.[12-18] These models primarily use porous electrode theory[19,20] to describe the porous nature of the electrode/separator and concentration solution theory to treat the transport processes in the electrolyte phase. The thermodynamics and kinetics of the reactions at the electrode/electrolyte interface are also described in these models in detail. Most of these models also account for the solid-phase diffusion of the active species into the bulk. While such detailed models throw light on the impedance behavior of systems when complicated by transport and kinetic processes, the mathematical interpretation is not straightforward.

In the list of comprehensive models developed to simulate the impedance behavior of lithium batteries, Doyle et al.[13] simulated the impedance response for a metal anode/separator/porous cathode system with all the above-mentioned details. Guo et al.[15] used a similar model to estimate the diffusion coefficient of lithium in carbon. Later, Dees et al.[18] included an electronically insulating oxide layer at the electrode/electrolyte interface to model a $LiNi_{0.8}Co_{0.15}Al_{0.05}O_2$ cathode. However, these models use a numerical scheme to solve for the variables to obtain the frequency domain impedance spectrum. There are also some analytical models[14,16,17] available in the literature, but they are not as comprehensive as the numerical models. Meyers et al.[14] presented an analytical solution to the impedance response of a porous electrode in the absence of solution-phase concentration gradients while Devan et al.[16] presented an analytical expression for the impedance response of a porous electrode limited to a symmetric cell, which included the solution-phase concentration gradients but neglected diffusion in the solid phase. In this work, we present an analytical expression for the impedance response of a metal foil/separator/insertion electrode system that includes the charge and mass balances in the solid and solution phases, with interfacial kinetics and double-layer adsorption. The analytical solution for the impedance of the cell, presented in this work is extremely useful for estimating transport and kinetic parameters and for the analysis of different limiting conditions. The analytical expression for the impedance response of the cell configuration used in this work can also be directly translated to any lithium metal rechargeable battery using insertion electrodes ($LiSOCl_2$, TiS_2, AgV_2O_5, etc.) and to insertion electrode half-cell systems.[3,21,22]

* Electrochemical Society Student Member.
** Electrochemical Society Fellow.
z E-mail: white@engr.sc.edu

Mathematical Model and Solution Technique

The cell configuration considered in this work (see Fig. 1) consists of a porous insertion electrode (cathode) and a metal foil (anode) separated by an ion conducting, but electronically insulating, separator. The porous electrode and the separator are flooded with electrolyte to facilitate the transport of ions in the solution phase. The model equations describing the porous electrode, separator, and the foil are similar to those of Doyle et al.[13] except that the active materials particles in the insertion electrode are assumed to be surrounded by an electronically insulating film. Hence, the interface between the particle and the solution phase is modeled by including internal interfacial impedance (electrode/film interface) and the impedance of the film.[14] The general electrochemical reaction at the insertion electrode is represented as

$$xM^+ + xe^- + \theta \underset{\text{deintercalation}}{\overset{\text{intercalation}}{\rightleftarrows}} M_x - \theta \qquad [1]$$

where x is the number of electrons transferred and θ is a vacant site for intercalation. In the foil electrode, the electrochemical reaction proceeds through a direct oxidation/reduction reaction at the electrode/solution interface. Although this model can be used for any insertion electrode systems, the model parameters and reactions scheme used in this work, typically, resembles a lithium insertion half-cell. The side reactions are ignored in this model.

The governing equations are treated with the standard procedures (linearizing about the open-circuit conditions, converting to Laplace domain, and finally, transforming to frequency space) employed in the literature.[16,23] The analytic expression for the impedance of the cell is derived by first solving for the Laplace transformed variables in the insertion electrode and then solving for the variables in the separator and the anode. The analytical solution for the impedance in the Laplace domain of the insertion electrode is coupled to the anode/separator through unknown constants.

Equations in the insertion electrode.— The governing equations (mass and charge balances in the solid and the solution phases) are presented in detail elsewhere[24] and the linearized equations (taking advantage of the small input perturbations) are presented here.

The material balance on the salt in the electrolyte is given by

$$\varepsilon_c \frac{\partial(c_c)}{\partial t} = \frac{\partial}{\partial x_c}\left(D_c^{\text{eff}} \frac{\partial c_c}{\partial x_c}\right) + \frac{a_c j_{n,c}(1 - t_+^0)}{\tilde{\upsilon}^+} \qquad [2]$$

The current densities in the solid and the electrolyte phases are expressed in the linear form as

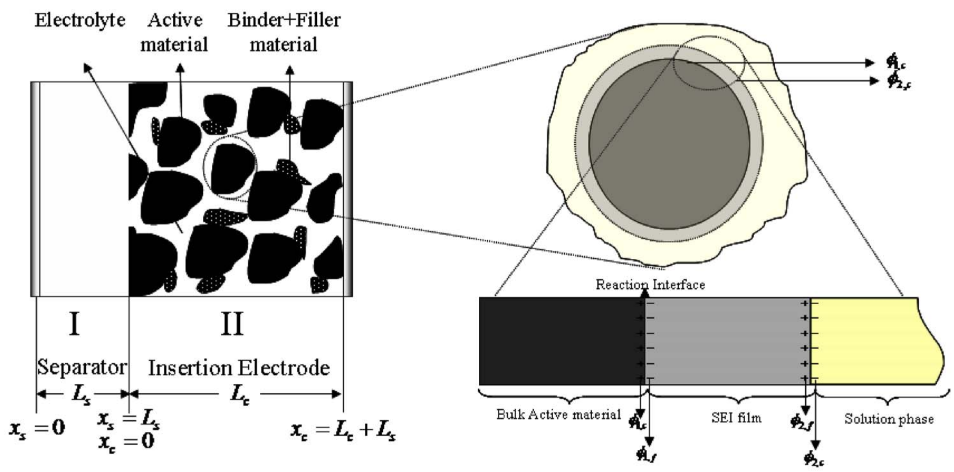

Figure 1. (Color online) Schematic of a foil/separator/porous insertion electrode cell sandwich. On the right: schematic of the magnified version of the interface showing the film at the electrode/electrolyte interface.

$$\mathbf{i}_{1,c} = -\sigma_c^{eff}\frac{\partial\phi_{1,c}}{\partial x_c} \quad [3]$$

$$\mathbf{i}_{2,c} = -\kappa_c^{eff}\left[\frac{\partial\phi_{2,c}}{\partial x_c} - \frac{2RT(1-t_+^0)}{F}\left(\frac{1}{c_B^0}+\frac{f'_{\pm,c_B^0}}{f_{\pm,c_B^0}}\right)\frac{\partial c_c}{\partial x_c}\right] \quad [4]$$

and the current transferred across the interface is related to the reaction flux as

$$\frac{\partial \mathbf{i}_{1,c}}{\partial x_c} = -Fa_c j_{n,c} \quad [5]$$

where $j_{n,c}$ is the flux transferred between the solution and the solid phase. The total current density transferred between the solution and the solid phase $(i_{n,c})$ is distributed between the film and the electrochemical interface through the possible current paths. The interface current density $(i_{int,c})$ is the sum of the contributions from the Faradaic current density $(i_{F,c})$ and the electrochemical double-layer current density $(i_{dl,c})$, which are given in the linearized form as

$$i_{F,c} = i_{o,c}\frac{(\alpha_{a,c}+\alpha_{c,c})F}{RT}\left[\phi_{1,c}-\phi_{1,f}-\left(\left.\frac{\partial U_c}{\partial c_\theta}\right|_{c_\theta^0}\right)c_\theta|_{r_c=R_p}\right] \quad [6]$$

$$i_{dl,c} = C_{dl,c}\frac{\partial}{\partial t}(\phi_{1,c}-\phi_{1,f}) \quad [7]$$

where $\phi_{1,f}$ is the potential in the film close to the solid phase and is related to the solution phase potential $\phi_{2,c}$ by the relation

$$\phi_{1,f} = \phi_{2,c} + (i_{dl,c} + i_{F,c})R_{film} \quad [8]$$

and $(\partial U_c/\partial c_\theta)|_{c_\theta^0}$ is the derivative of the open-circuit potential with respect to the solid-phase concentration at the initial concentration. The total current density $(i_{n,c})$ includes the contribution from the capacitance of the film in addition to the interfacial current density $(i_{int,c})$:

$$i_{n,c} = i_{F,c} + i_{dl,c} + C_{film,c}\frac{\partial}{\partial t}(\phi_{1,c}-\phi_{2,c}) \quad [9]$$

The diffusion of the active species in the spherical particle is assumed to obey Fick's law and is mathematically given by

$$\frac{\partial c_{\theta,c}}{\partial t} = \frac{D_{\theta,c}}{r_c^2}\frac{\partial}{\partial r_c}\left(r_c^2\frac{\partial c_{\theta,c}}{\partial r_c}\right) \quad [10]$$

The boundary conditions, for each of the variables to be solved in the insertion electrode $(c_c, \phi_{1,c}, \phi_{2,c})$, are given by

$$x_c = L_c + L_s: \quad D_c^{eff}\frac{\partial c_c}{\partial x_c} = 0; \quad \kappa_c^{eff}\frac{\partial\phi_{2,c}}{\partial x_c} = 0; \quad \sigma_c^{eff}\frac{\partial\phi_{1,c}}{\partial x_c} = -i_{app}$$

$$x_c = L_s: \quad D_c^{eff}\frac{\partial c_c}{\partial x_c} = \xi^*(t);$$

$$-\kappa_c^{eff}\left[\frac{\partial\phi_{2,c}}{\partial x_c} - \frac{2RT(1-t_+^0)}{F}\left(\frac{1}{c_B^0}+\frac{f'_{\pm,c_B^0}}{f_{\pm,c_B^0}}\right)\frac{\partial c_c}{\partial x_c}\right] = i_{app};$$

$$\sigma_c^{eff}\frac{\partial\phi_{1,c}}{\partial x_c} = 0 \quad [11]$$

and for the variable in the solid phase,$c_{\theta,c}$ is given by

$$r_c = 0: \quad D_{\theta,c}\frac{\partial c_{\theta,c}}{\partial r_c} = 0$$

$$r_c = R_p: \quad -D_{\theta,c}\frac{\partial c_{\theta,c}}{\partial r_c} = j_{F,c} = \frac{i_{F,c}}{nF} \quad [12]$$

Equations 2-5 with the boundary conditions in Eq. 11, represent the variables in the macroscale (along the thickness of the porous electrode, x_c) while Eq. 10 along with the boundary condition 12 represents the microscale solid-phase diffusion in a single spherical particle. The macroscale equations are coupled to the microscale Eq. 10 through the variable, $c_\theta|_{r_c=R_p}$ (the solid-phase concentrations at the surface) in Eq. 6. To determine the impedance response, the time domain equations are converted to the Laplace domain, and in the process the particle impedance (in the Laplace domain) can be solved independently, without solving for the other variables in the porous electrode. In this model the impedance of the particle can be obtained by solving Eq. 10 with the boundary conditions in Eq. 12, which allows us to relate the surface concentration to the faradaic current as[14]

$$\tilde{c}_{\theta,c}|_{r_c=R_p} = -\left(\frac{R_p}{D_{\theta,c}Y_s}\right)\tilde{j}_{F,c} \quad [13]$$

where the tilde is used to represent the variables in the Laplace domain. Furthermore, $\tilde{j}_{F,c}$ has the term $\tilde{\phi}_{1,f}$, which is eliminated using Eq. 8, and the total flux transferred between the solution and the matrix phase $(\tilde{j}_{n,c})$ in terms of the solid- and solution-phase potential is obtained by combining Eq. 6-9 and 13 as

$$\tilde{j}_{n,c} = \beta(\tilde{\phi}_{1,c} - \tilde{\phi}_{2,c}) \quad [14]$$

where $1/\beta F$ is the impedance of a single particle with a film and β is given by

$$\beta = \frac{1}{F}\left(sC_{\text{film}} + \frac{1}{\dfrac{1}{sC_{\text{dl}} + \dfrac{1}{R_{\text{ct}} + \dfrac{R_{\text{dif}}}{Y_{\text{s}}}}} + R_{\text{film}}} \right) \quad [15]$$

Here R_{dif} and R_{ct} represents the solid-phase diffusion and charge transfer resistances, respectively. The transfer function Y_{s} in Eq. 15 is given by[14]

$$Y_{\text{s}} = \frac{\sqrt{\dfrac{sR_p^2}{D_{\theta,\text{c}}}} - \tanh\left(\sqrt{\dfrac{sR_p^2}{D_{\theta,\text{c}}}}\right)}{\tanh\left(\sqrt{\dfrac{sR_p^2}{D_{\theta,\text{c}}}}\right)} \quad [16]$$

Expression 14 includes the impedance contributions from the particle, interface, and film and will be incorporated into Eq. 2-4 to describe the impedance in the porous electrode.

To solve for the impedance in the porous electrode, Eq. 2-4 are transformed using the dimensionless variables $\bar{c}_{\text{c}}, \bar{\eta}_{\text{c}}, \bar{x}_{\text{c}}, \bar{t}_{\text{c}}$ where

$$\bar{c}_{\text{c}} = -\frac{2RT(1-t_+^0)}{Fi_{\text{app}}}\left(\frac{1}{c_B^0} + \frac{f'_{\pm,c_B^0}}{f_{\pm,c_B^0}}\right)\frac{\sigma_{\text{c}}^{\text{eff}}}{L_{\text{c}}}(c_{\text{c}} - c_B^0),$$

$$\bar{\eta}_{\text{c}} = -\frac{\sigma_{\text{c}}^{\text{eff}}}{L_{\text{c}}}\left(\frac{\phi_{1,\text{c}} - \phi_{2,\text{c}}}{i_{\text{app}}}\right), \quad \bar{x}_{\text{c}} = \frac{x_{\text{c}} - L_{\text{s}}}{L_{\text{c}}}, \quad \bar{t}_{\text{c}} = \left(\frac{D_{\text{c}}^{\text{eff}}}{L_{\text{c}}^2\varepsilon_{\text{c}}}\right)t \quad [17]$$

and the resulting linear time-dependent partial differential equations are converted to the Laplace domain yielding two ordinary differential equations (Eq. 18 and 19), which describes the solution-phase concentration and overpotential in the insertion electrode

$$\frac{d^2\tilde{\bar{c}}_c}{d\bar{x}_{\text{c}}^2} = \bar{s}_{\text{c}}\tilde{\bar{c}}_{\text{c}} - \Theta_1\tilde{\bar{\eta}}_{\text{c}} \quad [18]$$

$$\frac{d^2\tilde{\bar{\eta}}_{\text{c}}}{d\bar{x}_{\text{c}}^2} = -\bar{s}_{\text{c}}\tilde{\bar{c}}_{\text{c}} + (\Theta_1 + \Theta_2)\tilde{\bar{\eta}}_{\text{c}} \quad [19]$$

The corresponding boundary conditions for the concentration and the potential at the insertion electrode/current collector interface and the electrode/separator interface are obtained by transforming Eq. 11 to the dimensionless form using the variables defined in Eq. 17 and converting to the Laplace domain

$$\bar{x}_{\text{c}} = 0: \quad \frac{d\tilde{\bar{c}}_{\text{c}}}{d\bar{x}_{\text{c}}} = -\frac{\Theta_1}{\Theta_2}\frac{F\left(1 + \dfrac{\sigma_{\text{c}}^{\text{eff}}}{\kappa_{\text{c}}^{\text{eff}}}\right)}{i_{\text{app}}(1-t_+^0)}\xi^*(\bar{s}_{\text{c}}), \quad \frac{d\tilde{\bar{\eta}}_{\text{c}}}{d\bar{x}_{\text{c}}} + \frac{d\tilde{\bar{c}}_{\text{c}}}{d\bar{x}_{\text{c}}} = -\left(\frac{\sigma_{\text{c}}^{\text{eff}}}{\kappa_{\text{c}}^{\text{eff}}}\right)$$

$$\bar{x}_{\text{c}} = 1: \quad \frac{d\tilde{\bar{c}}_{\text{c}}}{d\bar{x}_{\text{c}}} = 0, \quad \frac{d\tilde{\bar{\eta}}_{\text{c}}}{d\bar{x}_{\text{c}}} = 1 \quad [20]$$

It is worth noting that the concentration flux at the insertion electrode/separator interface (boundary condition at $\bar{x}_{\text{c}} = 0$) is coupled to the concentration flux in the separator boundary. However, this is a function of time alone and is represented as $\xi^*(t)$ in Eq. 11. This unknown time-dependent variable $\xi^*(t)$, when converted to the Laplace domain, yields an unknown function $\xi^*(\bar{s}_{\text{c}})$ in terms of the dimensionless Laplace variable $\bar{s}_{\text{c}}$. This simplifies the process of determining the analytical solution in the insertion electrode, because $\xi^*(\bar{s}_{\text{c}})$ is assumed to be a constant (unknown), which later is calculated by solving for the concentration in the separator region. [$\xi^*(\bar{s}_{\text{c}})$ can be assumed to be a constant while evaluating the impedance for a particular frequency because of the relation $s = j\omega$].

The solution to the coupled second-order differential Eq. 18 and 19 is given by[25]

$$\begin{bmatrix} \tilde{\bar{c}}_{\text{c}} \\ \tilde{\bar{\eta}}_{\text{c}} \end{bmatrix} = \begin{bmatrix} V_{1,1} \\ V_{2,1} \end{bmatrix}\begin{bmatrix} C_1 \cosh\sqrt{\lambda_1}\bar{x}_{\text{c}} + C_2 \sinh\sqrt{\lambda_1}\bar{x}_{\text{c}} \\ C_1 \cosh\sqrt{\lambda_1}\bar{x}_{\text{c}} + C_2 \sinh\sqrt{\lambda_1}\bar{x}_{\text{c}} \end{bmatrix} + \begin{bmatrix} V_{1,2} \\ V_{2,2} \end{bmatrix} \times \begin{bmatrix} C_3 \cosh\sqrt{\lambda_2}\bar{x}_{\text{c}} + C_4 \sinh\sqrt{\lambda_2}\bar{x}_{\text{c}} \\ C_3 \cosh\sqrt{\lambda_2}\bar{x}_{\text{c}} + C_4 \sinh\sqrt{\lambda_2}\bar{x}_{\text{c}} \end{bmatrix} \quad [21]$$

where

$$\begin{bmatrix} V_{1,1} \\ V_{2,1} \end{bmatrix} \text{ and } \begin{bmatrix} V_{1,2} \\ V_{2,2} \end{bmatrix}$$

are the eigenvectors corresponding to the eigenvalues λ_1 and λ_2, respectively. The eigenvalues are given by

$$\lambda_1 = \tfrac{1}{2}\left(\bar{s}_{\text{c}} + \Theta_1 + \Theta_2 + \sqrt{\bar{s}_{\text{c}}^2 + 2\Theta_1\bar{s}_{\text{c}} - 2\Theta_2\bar{s}_{\text{c}} + \Theta_1^2 + 2\Theta_1\Theta_2 + \Theta_2^2}\right)$$

$$\lambda_2 = \tfrac{1}{2}\left(\bar{s}_{\text{c}} + \Theta_1 + \Theta_2 - \sqrt{\bar{s}_{\text{c}}^2 + 2\Theta_1\bar{s}_{\text{c}} - 2\Theta_2\bar{s}_{\text{c}} + \Theta_1^2 + 2\Theta_1\Theta_2 + \Theta_2^2}\right) \quad [22]$$

and the eigenvectors can be written in terms of eigenvalues as

$$\begin{bmatrix} V_{1,1} \\ V_{2,1} \end{bmatrix} = \begin{bmatrix} 1 \\ \dfrac{\bar{s}_{\text{c}} - \lambda_1}{\Theta_1} \end{bmatrix}, \quad \begin{bmatrix} V_{1,2} \\ V_{2,2} \end{bmatrix} = \begin{bmatrix} 1 \\ \dfrac{\bar{s}_{\text{c}} - \lambda_2}{\Theta_1} \end{bmatrix} \quad [23]$$

The constants C_1, C_2, C_3, and C_4 are evaluated using the boundary conditions in Eq. 20.

$$C_1 = \frac{-\Theta_1}{\sqrt{\lambda_1}(\lambda_1 - \lambda_2)\sinh\sqrt{\lambda_1}} - \frac{C_2}{\tanh\sqrt{\lambda_1}}$$

$$C_2 = -\frac{\xi^*(\bar{s}_{\text{c}})}{i_{\text{app}}}\frac{\sigma_{\text{c}}^{\text{eff}}\Theta_1(\bar{s}_{\text{c}} - \lambda_2 + \Theta_1)}{\sqrt{\lambda_1}(\lambda_1 - \lambda_2)L_{\text{c}}^2 a_{\text{c}}(1-t_+^0)\beta} + \frac{\sigma_{\text{c}}^{\text{eff}}\Theta_1}{\kappa_{\text{c}}^{\text{eff}}\sqrt{\lambda_1}(\lambda_1 - \lambda_2)}$$

$$C_3 = \frac{\Theta_1}{\sqrt{\lambda_2}(\lambda_1 - \lambda_2)\sinh\sqrt{\lambda_2}} - \frac{C_4}{\tanh\sqrt{\lambda_2}} \quad [24]$$

$$C_4 = \frac{\xi^*(\bar{s}_{\text{c}})}{i_{\text{app}}}\frac{\sigma_{\text{c}}^{\text{eff}}\Theta_1(\bar{s}_{\text{c}} - \lambda_1 + \Theta_1)}{\sqrt{\lambda_2}(\lambda_1 - \lambda_2)L_{\text{c}}^2 a_{\text{c}}(1-t_+^0)\beta} - \frac{\sigma_{\text{c}}^{\text{eff}}\Theta_1}{\kappa_{\text{c}}^{\text{eff}}\sqrt{\lambda_2}(\lambda_1 - \lambda_2)}$$

Plugging in the expressions of the constants (C_1, C_2, C_3, and C_4) into Eq. 21 yields the analytical expressions for the Laplace transformed dimensionless concentration and potential in the insertion electrode. However, the value of $\xi^*(\bar{s}_{\text{c}})$ is still an unknown and is evaluated by solving for the variables in the separator region.

Equations in the separator.— The governing equations for the solution-phase concentration and potential in the separator region are given by (in linearized form)

$$\frac{\partial(\varepsilon_{\text{s}}c_{\text{s}})}{\partial t} = \frac{\partial}{\partial x_{\text{s}}}\left(D_{\text{s}}^{\text{eff}}\frac{\partial c_{\text{s}}}{\partial x_{\text{s}}}\right) \quad [25]$$

$$i_{\text{app}} = -\kappa_{\text{s}}^{\text{eff}}\left[\frac{\partial\phi_{2,\text{s}}}{\partial x_{\text{s}}} - \frac{2RT(1-t_+^0)}{F}\left(\frac{1}{c_B^0} + \frac{f'_{\pm,c_B^0}}{f_{\pm,c_B^0}}\right)\frac{\partial c_{\text{s}}}{\partial x_{\text{s}}}\right] \quad [26]$$

and the boundary conditions for each of the variables are

$$x_{\text{s}} = 0: \quad D_{\text{s}}^{\text{eff}}\frac{\partial c_{\text{s}}}{\partial x_{\text{s}}} = \frac{-i_{\text{app}}(1-t_+^0)}{F}, \quad x_{\text{s}} = L_{\text{s}}: \quad D_{\text{s}}^{\text{eff}}\frac{\partial c_{\text{s}}}{\partial x_{\text{s}}} = \xi^*(t)$$

$$x_{\text{s}} = L_{\text{s}}: \quad \phi_{2,\text{s}} = 0, \quad \text{reference point} \quad [27]$$

The absence of reaction in the separator region provides a way to solve for the solution-phase concentration profile independently of the potential, as seen from Eq. 25 and 26. Introducing the dimensionless variables

$$\bar{c}_s = \frac{c_s - c_B^0}{c_B^0}, \quad \bar{x}_s = \frac{x_s}{L_s}, \quad \bar{t} = \left(\frac{D_s^{eff}}{L_s^2 \varepsilon_s}\right) t \qquad [28]$$

and converting Eq. 25-27 to the Laplace domain yields

$$\frac{\partial \tilde{\phi}_{2,s}}{\partial \bar{x}_s} = -L_s \frac{i_{app}}{\kappa_s^{eff}} + \Theta_3 \frac{\partial \tilde{\bar{c}}_s}{\partial \bar{x}_s} \qquad [30]$$

$$\bar{x}_s = 1, \quad \tilde{\phi}_{2,s} = 0 \qquad [31]$$

The solution for Eq. 29 with the corresponding boundary conditions in Eq. 31 yields

$$\tilde{\bar{c}}_s = C_5 \cosh \sqrt{\bar{s}_s}\bar{x}_s + C_6 \sinh \sqrt{\bar{s}_s}\bar{x}_s \qquad [32]$$

where

$$C_5 = \frac{L_s}{D_s^{eff} c_B^0 \sqrt{\bar{s}_s}}\left(\frac{\xi^*(\bar{s}_s)}{\sinh \sqrt{\bar{s}_s}} + \frac{i_{app}(1 - t_+^0)}{F \tanh \sqrt{\bar{s}_s}}\right), \quad C_6 = -\frac{i_{app}(1 - t_+^0)L_s}{D_s^{eff} F c_B^0 \sqrt{\bar{s}_s}} \qquad [33]$$

Since the concentrations are continuous across the separator/insertion electrode boundary, expressions 32 and 21 can be used to evaluate ξ^*

$$(c_B^0)\, \tilde{\bar{c}}_s|_{\bar{x}_s=1} = \left(-\frac{\Theta_2}{\Theta_1} \frac{L_c i_{app}(1 - t_+^0)}{D_c^{eff} \tilde{\upsilon}^+ F\left(1 + \frac{\sigma_c^{eff}}{\kappa_c^{eff}}\right)} \xi^*(\bar{s}_c)\right) \tilde{\bar{c}}_c|_{\bar{x}_c=0} \qquad [34]$$

which yields

$$(c_B^0)(C_5 \cosh \sqrt{\bar{s}_s} + C_6 \sinh \sqrt{\bar{s}_s}) = \left(-\frac{\Theta_2}{\Theta_1} \frac{L_c i_{app}(1 - t_+^0)}{D_c^{eff} \tilde{\upsilon}^+ F\left(1 + \frac{\sigma_c^{eff}}{\kappa_c^{eff}}\right)} \xi^*(\bar{s}_c)\right)(C_1 + C_3) \qquad [35]$$

Equation 35 can be turned around to solve explicitly for ξ^*

$$i_{app} = \left[i_{o,a}F\left(\frac{\alpha_{a,a} + \alpha_{c,a}}{RT}\right) + \bar{s}_a C_{dl,a}\right](\tilde{\phi}_{1,a}|_{\bar{x}_s=0} - \tilde{\phi}_{2,s}|_{\bar{x}_s=0}) \qquad [38]$$

The solution-phase potential $\phi_{2,s}$ at $\bar{x}_s = 0$ is obtained from expression 37 to be

$$\tilde{\phi}_{2,s}|_{\bar{x}_s=0} = L_s \frac{i_{app}}{\kappa_s^{eff}} + \Theta_3(\tilde{\bar{c}}_s|_{\bar{x}_s=0} - \tilde{\bar{c}}_s|_{\bar{x}_s=1}) \qquad [39]$$

The value for $(\tilde{\bar{c}}_s|_{\bar{x}_s=0} - \tilde{\bar{c}}_s|_{\bar{x}_s=1})$ can be obtained from Eq. 32 and 39 becomes

$$\tilde{\phi}_{2,s}|_{\bar{x}_s=0} = L_s \frac{i_{app}}{\kappa_s^{eff}} + \Theta_3[C_5(1 - \cosh \sqrt{\bar{s}_s}) - C_6 \sinh \sqrt{\bar{s}_s}] \qquad [40]$$

which can be simplified to

$$\tilde{\phi}_{2,s}|_{\bar{x}_s=0} = L_s \frac{i_{app}}{\kappa_s^{eff}} + \frac{\Theta_3 L_s}{D_s^{eff} c_B^0 \sqrt{\bar{s}_s}}\left(\xi^*(\bar{s}_s) - \frac{i_{app}(1 - t_+^0)}{F}\right)\left(\frac{1}{\sinh \sqrt{\bar{s}_s}} - \frac{1}{\tanh \sqrt{\bar{s}_s}}\right) \qquad [41]$$

Equation 41 can be plugged into Eq. 38 which can be solved for the potential at the foil to yield

$$\tilde{\phi}_{1,a}|_{\bar{x}_s=0} = L_s \frac{i_{app}}{\kappa_s^{eff}} + \frac{\Theta_3 L_s}{D_s^{eff} c_B^0 \sqrt{\bar{s}_s}}\left(\xi^*(\bar{s}_s) - \frac{i_{app}(1 - t_+^0)}{F}\right)\left(\frac{1}{\sinh \sqrt{\bar{s}_s}} - \frac{1}{\tanh \sqrt{\bar{s}_s}}\right) + \frac{i_{app}}{i_{o,a}F\left(\frac{\alpha_{a,a} + \alpha_{c,a}}{RT}\right) + \bar{s}_a C_{dl,a}} \qquad [42]$$

$$\xi^* = \frac{i_{app}(1 - t_+)\left\{\frac{L_s}{\sqrt{\bar{s}_s} D_s^{eff} F \sinh \sqrt{\bar{s}_c}} + \frac{L_c^3 a_c \beta}{\sigma_c^{eff} D_c^{eff}(\lambda_1 - \lambda_2)}\left(\begin{array}{l}\left[\frac{1}{\sqrt{\lambda_2} \sinh \sqrt{\lambda_2}} - \frac{1}{\sqrt{\lambda_1} \sinh \sqrt{\lambda_1}}\right] - \frac{\sigma_c^{eff}}{\kappa_c^{eff}} \\ \left[\frac{1}{\sqrt{\lambda_1} \tanh \sqrt{\lambda_1}} - \frac{1}{\sqrt{\lambda_2} \tanh \sqrt{\lambda_2}}\right]\end{array}\right)\right\}}{\frac{L_c}{D_c^{eff}(\lambda_1 - \lambda_2)}\left(\frac{\bar{s}_c - \lambda_1 + \Theta_1}{\sqrt{\lambda_2} \tanh \sqrt{\lambda_2}} - \frac{\bar{s}_c - \lambda_2 + \Theta_1}{\sqrt{\lambda_1} \tanh \sqrt{\lambda_1}}\right) - \frac{L_s}{\sqrt{\bar{s}_c} D_s^{eff} \tanh \sqrt{\bar{s}_c}}} \qquad [36]$$

To solve for the potential in the separator region Eq. 30 is integrated, and the reference point, $\tilde{\phi}_{2,s} = 0$ at $\bar{x}_s = 1$ is used to eliminate the integration constant, which yields

$$\tilde{\phi}_{2,s} = L_s \frac{i_{app}}{\kappa_s^{eff}}(1 - \bar{x}_s) + \Theta_3(\tilde{\bar{c}}_s - \tilde{\bar{c}}_s|_{\bar{x}_s=1}) \qquad [37]$$

Equations in the foil.— The current density crossing the solution phase/foil interface is either due to the Faradaic reaction (which follows Butler–Volmer kinetics) or due to the charging/discharging of the electrochemical double layer. The linearized expression for the current density transferred across the interface due to the Faradaic and double-layer processes in the Laplace domain is given by

Impedance of the insertion electrode.— The impedance of the insertion electrode is given by

$$Z_c = -\frac{\tilde{\phi}_{1,c}|_{\bar{x}_c=1} - \tilde{\phi}_{2,s}|_{\bar{x}_s=1}}{i_{app}} \qquad [43]$$

We have defined $\tilde{\phi}_{2,s}|_{\bar{x}_s=1} = 0$ (see Eq. 31) and $\tilde{\phi}_{1,c}|_{\bar{x}_c=1}$ is obtained by integrating the solution for the over potential (Eq. 21). Combining Eq. 3 with 5, and writing $j_{n,c}$ in terms of the overpotential through Eq. 14 followed by nondimensionalizing through Eq. 17, we obtain

$$\frac{d^2 \tilde{\phi}_{1,c}}{d\bar{x}_c^2} = \left(-\frac{L_c^3 a_c F \beta i_{app}}{\sigma_c^{eff^2}}\right)\tilde{\bar{\eta}}_c \qquad [44]$$

which on integration yields

$$\tilde{\phi}_{1,c} = \left(-\frac{L_c^3 a_c F \beta i_{app}}{\sigma_c^{eff^2}}\right) \int\int \tilde{\tilde{\eta}}_c d\bar{x}_c d\bar{x}_c + C_7 \bar{x}_c + C_8 \quad [45]$$

where C_7 and C_8 are eliminated using the conditions

$$\bar{x}_c = 0, \quad \tilde{\phi}_{1,c} = -\frac{L_c i_{app}}{\sigma_c^{eff}} \tilde{\tilde{\eta}}_c|_{\bar{x}_c=0}, \quad \bar{x}_c = 1, \frac{d\tilde{\phi}_{1,c}}{d\bar{x}_c} = -\frac{L_c i_{app}}{\sigma_c^{eff}} \quad [46]$$

and the constants C_7 and C_8 are evaluated to be

$$C_7 = -\frac{L_c i_{app}}{\sigma_c^{eff}}\left(1 - \frac{L_c^2 a_c F \beta \bar{s}_c}{\sigma_c^{eff}\lambda_1\lambda_2}\right)$$

$$C_8 = -\frac{L_c i_{app}}{\sigma_c^{eff}}\left[\frac{\bar{s}_c - \lambda_1}{\Theta_1}C_1\left(1 - \frac{L_c^2 a_c F\beta}{\sigma_c^{eff}\lambda_1}\right) + \frac{\bar{s}_c - \lambda_2}{\Theta_1}C_3\left(1 - \frac{L_c^2 a_c F\beta}{\sigma_c^{eff}\lambda_2}\right)\right] \quad [47]$$

Substituting the values of the constants in Eq. 45 the impedance of the cathode is obtained as

$$Z_c = \frac{L_c}{\sigma_c^{eff} + \kappa_c^{eff}} + \frac{L_c^3 a_c F\beta}{\sigma_c^{eff^2}\Theta_1}\left\{\frac{\bar{s}_c - \lambda_1}{\lambda_1}\left(\frac{-\Theta_1}{\sqrt{\lambda_1}(\lambda_1 - \lambda_2)\tanh\sqrt{\lambda_1}} - \frac{C_2}{\sinh\sqrt{\lambda_1}}\right) + \frac{\bar{s}_c - \lambda_2}{\lambda_2}\left(\frac{\Theta_1}{\sqrt{\lambda_2}(\lambda_1 - \lambda_2)\tanh\sqrt{\lambda_2}} - \frac{C_4}{\sinh\sqrt{\lambda_2}}\right) + \frac{\bar{s}_c - \lambda_1}{\lambda_1}C_1\left(\frac{\sigma_c^{eff}\lambda_1}{L_c^2 a_c F\beta} - 1\right) + \frac{\bar{s}_c - \lambda_2}{\lambda_2}C_3\left(\frac{\sigma_c^{eff}\lambda_2}{L_c^2 a_c F\beta} - 1\right)\right\} \quad [48]$$

Impedance of the full cell.— The impedance of the full cell is given by

$$Z_{cell} = -\frac{\tilde{\phi}_{1,c}|_{\bar{x}_c=1} - \tilde{\phi}_{1,a}|_{\bar{x}_s=0}}{i_{app}} \quad [49]$$

which includes the impedance contributions from the separator and the foil anode along with the insertion electrode. Substituting in the expressions for $\tilde{\phi}_{1,c}|_{\bar{x}_c=1}$ and $\tilde{\phi}_{1,a}|_{\bar{x}_s=0}$ from Eq. 48 and 42, respectively, in Eq. 49

$$Z_{cell} = \left[\underbrace{\left\{\frac{L_s}{\kappa_s^{eff}} + \frac{L_c}{\sigma_c^{eff} + \kappa_c^{eff}}\right\}}_{\mathrm{I}} + \underbrace{\frac{L_c^3 a_c F\beta}{\sigma_c^{eff^2}\Theta_1}\left\{\frac{\bar{s}_c - \lambda_1}{\lambda_1}\left(\frac{-\Theta_1}{\sqrt{\lambda_1}(\lambda_1 - \lambda_2)\tanh\sqrt{\lambda_1}} - \frac{C_2}{\sinh\sqrt{\lambda_1}}\right) + \frac{\bar{s}_c - \lambda_2}{\lambda_2}\left(\frac{\Theta_1}{\sqrt{\lambda_2}(\lambda_1 - \lambda_2)\tanh\sqrt{\lambda_2}} - \frac{C_4}{\sinh\sqrt{\lambda_2}}\right) + \frac{\bar{s}_c - \lambda_1}{\lambda_1}C_1\left(\frac{\sigma_c^{eff}\lambda_1}{L_c^2 a_c F\beta} - 1\right) + \frac{\bar{s}_c - \lambda_2}{\lambda_2}C_3\left(\frac{\sigma_c^{eff}\lambda_2}{L_c^2 a_c F\beta} - 1\right)\right\}}_{\mathrm{II}} + \underbrace{\frac{\Theta_3 L_s}{D_s^{eff} c_B^0 \sqrt{\bar{s}_s}}\left(\frac{\xi^*(\bar{s}_s)}{i_{app}} - \frac{1 - t_+^0}{F}\right)\left(\frac{1}{\sinh\sqrt{\bar{s}_s}} - \frac{1}{\tanh\sqrt{\bar{s}_s}}\right)}_{\mathrm{III}} + \frac{1}{\underbrace{i_{o,a}F\left(\frac{\alpha_{a,a} + \alpha_{c,a}}{RT}\right) + \bar{s}_a C_{dl,a}}_{\mathrm{IV}}}\right] \quad [50]$$

Results and Discussion

The impedance response was simulated for a $LiCoO_2$ insertion cathode with a Li foil anode and a polypropylene separator. The impedance solution predicted using the analytical expression was verified by comparing with the numerical solution obtained for the same model using Comsol MultiPhysics®. Figure 2 shows the comparison of the analytical solution for the impedance of the cell from Eq. 50 and the corresponding numerical solution for different states of charge using the parameter values shown in Table I. The results obtained through the analytical solution agree well with the numerical solution over the complete range of simulated frequencies. The impedance spectrum shown in Fig. 2 is the cumulative response from the anode, cathode, and the separator and reveals a high-frequency arc, which is caused by the resistance and the capacitance of the film and a midfrequency arc, which is the contribution from the charge-transfer/double-layer process at the electrochemical interface. At low frequencies, the impedance spectrum consists of the effects due to solid-phase diffusion, usually characterized by a 45° asymptote originating from the real axis, which is also referred to as the Warburg impedance. However, in this case the Warburg region of the impedance spectrum is complicated by the solution-phase diffusion processes, and affects the 45° asymptote originating from the real axis, as seen in Fig. 2 and in the phase plots in Fig. 3. At very low frequencies, the impedance is due to the emptying/filling of the active species in the solid particle without concentration gradients within the particle. Thus, a capacitor-type impedance response can be seen at such low frequencies. The magnitude of the imaginary part of the low-frequency impedance depends on the change in the value of the open-circuit potential of the insertion electrode with respect to the concentration of active species ($\partial U_c/\partial c_\theta$) in the insertion electrode. The low-frequency tail is not observed when $\partial U_c/\partial c_\theta = 0$. The change in the impedance spectrum with state of charge can be characterized by the change in the low-frequency behavior, especially in the semi-infinite and finite-diffusion regions. While the magnitude of the high- and midfrequency part of the spectrum does not change with state of charge, the low-frequency impedance significantly increases with decrease in state of charge. This is because of the increase in value of $-\partial U_c/\partial c_\theta$ at lower states of charge (as marked), which increases the diffusional resistance, R_{dif}.

From the analytical expression, the total impedance of the cell can be split into four major parts: term (I), marked in Eq. 50, corresponds to the Ohmic resistances from the separator and the inser-

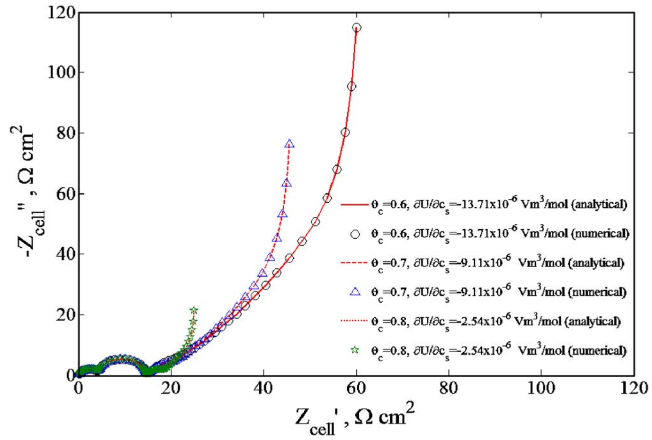

Figure 2. (Color online) Complex plane impedance plot showing the comparison of the cell impedance, Z_{cell} obtained from the analytical solution and numerical solution for different states of charge, θ_c. The analytical values are represented by lines while the numerical values are represented by symbols. The terms Z'_{cell} and Z''_{cell} denote the real and the imaginary part of the impedance respectively. The impedance values were obtained at 100 evenly spaced logarithmic frequency points between 10^5 Hz and 5×10^{-4} Hz.

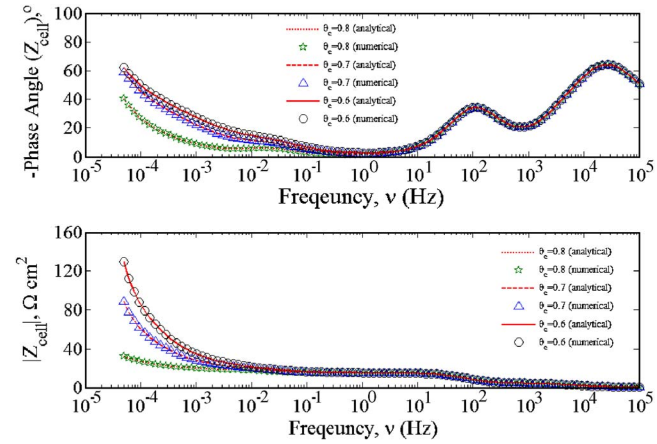

Figure 3. (Color online) Bode plots showing the phase difference and the magnitude of the impedance of the cell, $|Z_{\text{cell}}|$ against frequency, $\nu = \omega/2\pi$ obtained from the analytical solution and numerical solution for different states of charge, θ_c. The analytical values are represented by lines while the numerical values are represented by symbols. The values of the phase difference and magnitude were obtained at 100 evenly spaced logarithmic frequency points between 10^5 Hz and 5×10^{-4} Hz.

tion electrode. The resistance of the film is not separated out because the film capacitance is in parallel with the film resistance. Term (II) includes the contribution from the impedance of the electrochemical interface, film, and solution-phase and solid-phase diffusion in the insertion electrode, all added together. Term (III) is the contribution from diffusional impedance in the separator region and term (IV) corresponds to the interfacial impedance in the anode. Using the analytical solution, the impedance of the foil, separator, and the insertion electrode can also be separated out from the full cell. The isolation of the individual impedance from the analytical expression is very useful, especially when experimental data are obtained from different cell configurations. For instance, when a three-electrode setup is used to measure the impedance of the insertion cathode with respect to the reference electrode placed close to the insertion electrode/separator boundary, the impedance expression for the insertion electrode alone (Eq. 48) can be used for model/data comparison, and if the impedance data is taken on a two-electrode system the impedance expression for the full cell (Eq. 50) could be used. Figure 4 shows the impedance contribution of the individual components towards the overall cell impedance. It can be seen that for the parameter values used for this system, a significant part of the impedance spectrum of the cell arises from the impedance of the insertion electrode (Eq. 48). The impedance of the insertion electrode alone closely resembles the overall cell impedance and has contributions from the impedance of the film, charge-transfer/double-layer impedance of the electrochemical interface, and solid- and solution-phase diffusion impedances in the insertion electrode. The anode impedance shows a single arc in the high-frequency re-

Table I. Parameter values used in the model for $LiCoO_2$ cathode.

Parameters	Values
$D_{\theta,c}$ (m^2/s)	1×10^{-14} [a]
σ_c (S/m)	1×10^{2} [a]
c_T (mol/m^3)	5.1555×10^{4} [b]
$i_{0,a}$ (A/m^2)	1×10^{2} [a]
$i_{0,c}$ (A/m^2)	2 [a]
$\alpha_{a,c}$	0.5 [a]
$\alpha_{c,c}$	0.5 [a]
R_p (m)	10×10^{-6} [a]
ε_c	0.3 [b]
ε_c^f	0.18 [b]
$f_{\pm,c_B^0}$	1.2819 (Ref. 35)
$f'_{\pm,c_B^0}$ (m^3/mol)	1.47×10^{-3}(Ref. 35)
D_c (m^2/s)	3.208×10^{-10} [a]
L_c (m)	81×10^{-6} [b]
C_{film} (F/m^2)	1×10^{-2} [a]
R_{film} (Ωm^2)	2×10^{-3} [a]
$C_{dl,a}$ (F/m^2)	0.2 [a]
L_s (m)	25×10^{-6} [b]
ε_s	0.7 [a]
κ (S/m)	10.0 [a]
T (K)	298
c_B^0 (mol/m^3)	1×10^{3} [b]

[a] Assumed values.
[b] Measured values.

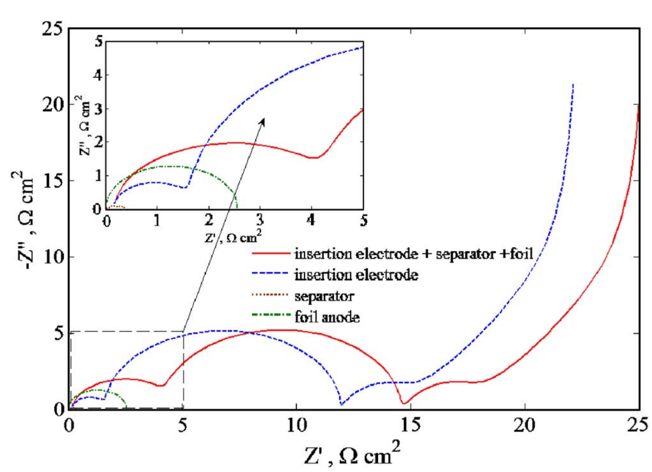

Figure 4. (Color online) Complex plane impedance plot showing the contribution of foil, separator and the insertion electrode towards the overall impedance of the cell, Z_{cell}. The terms Z' and Z'' denote the real and the imaginary part of the impedance respectively. Analytical expressions for each of these impedances are obtained from Eq. 47. The impedance values were obtained at 100 evenly spaced logarithmic frequency points between 10^5 Hz and 5×10^{-4} Hz at a state of charge, $\theta_c = 0.8$. Inset shows the zoomed version of the same plot to reveal the relatively small contribution of the foil anode and the separator towards the overall cell impedance.

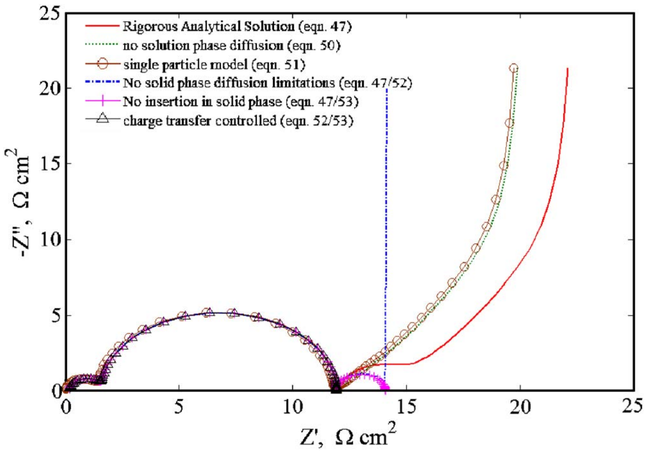

Figure 5. (Color online) Complex plane impedance plot showing the impedance spectrum of the insertion electrode, Z_c under different limiting conditions. The analytical solution for the impedance of the insertion electrode reduces to simpler expressions for different limiting conditions (as marked in the legends). The terms Z' and Z'' denote the real and the imaginary part of the impedance respectively. The impedance values were obtained at 100 evenly spaced logarithmic frequency points between 10^5 Hz and 5×10^{-4} Hz at a state of charge, $\theta_c = 0.8$.

gion corresponding to the charge-transfer resistance in parallel with the double-layer capacitance at the foil/electrolyte interface. The characteristic solid-phase diffusion limitations and the low-frequency capacitive behavior in the insertion electrode is absent in the anode because of the absence of insertion processes in the metal foil. The impedance contribution from the separator is the smallest of all these impedances and it shows two depressed semicircles partially overlapping each other (the spectrum lies very close to the origin and is seen better in the magnified inset in Fig. 4). Although we might expect a single time constant corresponding to the solution-phase diffusion in the separator region, the boundary conditions in the separator could have made the profiles complex. The impedance of the electrolyte filled porous separator should be similar to the diffusion impedance for a Nernstian or an impermeable boundary in a planar geometry,[26] however, it is complicated by the transient boundary at the separator/insertion electrode boundary.

Model versatility.— The versatility of the model is presented in Fig. 5, wherein the impedance spectrum of the insertion electrode is plotted for different limiting conditions that are often experimentally sustained. For illustration of the model versatility, the impedance spectrum of the insertion electrode alone was chosen. The solid line in Fig. 5 corresponds to the impedance response of the insertion electrode obtained using Eq. 48, which includes the impedance contribution from all the transport and kinetic processes. The dotted line corresponds to the case, when the solution-phase diffusion limitations are completely absent and are plotted using Eq. 51. For this condition, Eq. 48 can be reduced (based on the assumption $\lambda_1 \simeq \bar{s}_c$ and $\lambda_2 \simeq \Theta_2$) to the form (see Appendix A for derivation)

$$Z_c = \frac{L_c}{\sigma_c^{\text{eff}} + \kappa_c^{\text{eff}}}\left(1 + \frac{1}{\sqrt{\Theta_2}\tanh\sqrt{\Theta_2}}\left(\frac{\sigma_c^{\text{eff}}}{\kappa_c^{\text{eff}}} + \frac{\kappa_c^{\text{eff}}}{\sigma_c^{\text{eff}}}\right) + \frac{2}{\sqrt{\Theta_2}\sinh\sqrt{\Theta_2}}\right) \quad [51]$$

This expression is similar (with the exclusion of particle size distribution) to that presented by Meyers et al.[14] for a porous electrode without concentration gradients in the solution phase. A striking difference in the impedance spectrum (at the start of the Warburg region) when the solution-phase diffusion limitations were ignored is the suppression of the hump at the start of the Warburg region and a pure solid-phase diffusion behavior is observed. However, for the case when the solution-phase diffusion processes were included, there is a mixed control of the solution and solid-phase diffusion processes at the start of the Warburg region, which causes the hump. The extension of the impedance of the single particle to a porous electrode without solution-phase concentration gradients (with the Ohmic resistances added), given by $Z_{c,\text{part}}$, is also plotted in Fig. 5 for comparison

$$Z_{c,\text{part}} = \frac{L_c}{\sigma_c^{\text{eff}} + \kappa_c^{\text{eff}}} + \frac{1}{FL_c a_c \beta} \quad [52]$$

Equation 52 does not capture the nonuniformity of the current distribution in the porous electrode as compared to Eq. 51, however, the impedance spectrum obtained through either equations (51 or 52) are very similar for this system because of the small value of the parameter Θ_2, which controls the nonuniformity of the reaction distribution inside the porous electrode.[19] The depressed nature of the semicircle and the 45° asymptote at the high frequency, which are characteristic of porous electrodes,[27] are not obvious in the plot of Eq. 50 or 51 because of the high value of the charge transfer resistance. The 45° asymptote starts at very high frequencies and immediately merges into the part of the semicircle corresponding to charge transfer.

For the case when the system is unaffected by the solid-phase diffusion process, for instance, at very high values of solid-phase diffusion coefficient the transfer function in expression 16 reduces to[26]

$$\frac{1}{Y_s} = \frac{1}{5} + 3\frac{D_{\theta,c}}{sR_p^2} \quad [53]$$

In this case the impedance expression is given by Eq. 48 with the transfer function described in Eq. 53. It can be seen from Fig. 5 that the impedance for such a case is dominated by finite capacity effects in the low-frequency region and the Warburg-like solid-phase diffusion impedance is absent. At high and medium frequencies the impedance spectrum is dominated by Ohmic, charge transfer, and solution-phase diffusion resistances. It should be noted that the value chosen for the solution-phase diffusion coefficient is high so that the Warburg-like tail in the high-frequency region due to solution-phase diffusion process does not significantly extend into the lower frequencies and is suppressed by finite capacity effects. For the case when the solid-phase insertion is completely absent, then the diffusion inside the spherical particle does not exist, and hence, the expression for β in Eq. 15 reduces to

$$\beta = \frac{1}{F}\left(sC_{\text{film}} + \frac{sC_{\text{dl}} + \frac{1}{R_{ct}}}{1 + \left(sC_{\text{dl}} + \frac{1}{R_{ct}}\right)R_{\text{film}}}\right) \quad [54]$$

and the corresponding impedance response (Eq. 48 with the value of β from Eq. 54) is also shown in Fig. 5. The prominent features of this limiting condition are the absence of the diffusion tail and the finite capacity effects. This result is similar to the impedance spectrum obtained for a symmetric electrode configuration with the inclusion of solution-phase diffusion effects but without solid-phase diffusion limitations.[16] Finally, when the solution-phase and solid-phase diffusion limitations are dominated by the reaction kinetics, the impedance expression is obtained by using the expressions for β described in Eq. 54 along with Eq. 51 This reduces to the form described for the impedance of a resistor capacitor network.[28] The impedance spectrum is characterized by a very high- frequency arc corresponding to the film and another arc in the mid- and low-frequency range, corresponding to the charge-transfer/double-layer resistance.

Limiting cases.— Based on the analytical expression obtained for the impedance of the cell, useful expressions can be evaluated for different limiting cases. For the analyses of limiting conditions, the impedance response of the insertion electrode (described in Eq.

48) alone was considered. At high frequencies, the eigenvalues λ_1 and λ_2 reduce to $\lambda_1 \simeq \bar{s}_c$ and $\lambda_2 \simeq \Theta_2$ from expressions in Eq. 22. This is based on the same argument as for the case of the absence of solution-phase diffusion limitations (see Appendix A). Here, we assume that at significantly high frequencies the solution-phase diffusion processes have not yet started, and hence, Eq. 51 can accurately represent impedance behavior at high frequencies. In addition, the diffusion in the solid-phase can also be neglected at high frequencies, and hence, β (which occurs in Θ_2) can be reduced to the form in Eq. 54, which yields the impedance at high frequency (HF) as

$$Z_c^{HF} = \frac{L_c}{\sigma_c^{eff} + \kappa_c^{eff}}\left(1 + \frac{1}{\sqrt{\Theta_2^{HF}}\tanh\sqrt{\Theta_2^{HF}}}\left(\frac{\sigma_c^{eff}}{\kappa_c^{eff}} + \frac{\kappa_c^{eff}}{\sigma_c^{eff}}\right) + \frac{2}{\sqrt{\Theta_2^{HF}}\sinh\sqrt{\Theta_2^{HF}}}\right) \qquad [55]$$

where Θ_2 can be written as

$$\Theta_2^{HF} = L_c^2 a_c\left(\frac{1}{\sigma_c^{eff}} + \frac{1}{\kappa_c^{eff}}\right)\left(sC_{film} + \frac{sC_{dl} + \frac{1}{R_{ct}}}{1 + \left(sC_{dl} + \frac{1}{R_{ct}}\right)R_{film}}\right) \qquad [56]$$

The validity of this expression in the high-frequency region depends on the time constants of the solution-phase/solid-phase diffusion process.

In the low-frequency region, simplified expressions for the impedance of the cell would be very useful for estimating parameters such as solid-phase diffusion coefficient and solution-phase diffusion coefficient. Different analytical expressions to evaluate the solid-phase diffusion coefficient based on the slopes in the semi-infinite and transition region or the real part of the impedance extrapolated at zero frequencies in the finite diffusion region (low-frequency intercept technique) are available in the present literature. In most insertion electrode cells, the semi-infinite and the transition region are completely controlled by solid-phase diffusion process, and hence, the slope of these regions are widely used to determine solid-phase diffusion coefficients.[3,23,30] However, when the solution-phase processes overlap with the solid-phase processes in the semi-infinite/transition region a reliable estimate of the solid-phase diffusion coefficient (using standard formula[29]) is not guaranteed.[13] In the low-frequency intercept technique, the real part of the impedance extrapolated at zero frequencies is used to obtain the solid-phase diffusion coefficients[26,29] (extraction of diffusion coefficient from the finite-diffusion region of the impedance spectrum); although its applicability is limited by the fact that it requires longer times to obtain data at such low frequencies.[13,18] This method also cannot predict diffusion coefficient accurately using traditional expression when interference from solution-phase processes and the effects of porous electrode nature are prominent. In the work by Doyle et al.[13] the authors have concluded that the real part of the impedance extrapolated at zero frequencies from experimental data cannot be reliably used to measure diffusion coefficients in lithium rechargeable battery systems, because of the porous nature of the electrode and the interference of solution phase-diffusion processes with the solid-phase diffusion in the low-frequency regions; these are not captured by the analytic expressions in the literature (e.g, see Eq. 58). The analytical solution developed in this work (described in Eq. 48) includes the effect of solution-phase diffusion processes along with the solid-phase diffusion and finite capacity effects and is based on porous electrodes. Thus, the simplification of the impedance expression in Eq. 48 for low frequencies should yield a reliable analytic expression for the estimation of diffusion coefficient from the low-frequency intercept of the impedance spectrum. However, the direct simplification of Eq. 48 at low frequencies is cumbersome, and hence, the governing equations were solved by replacing the transient solution-phase diffusion equation with the steady-state diffusion equation to yield the low-frequency (LF) impedance expression as

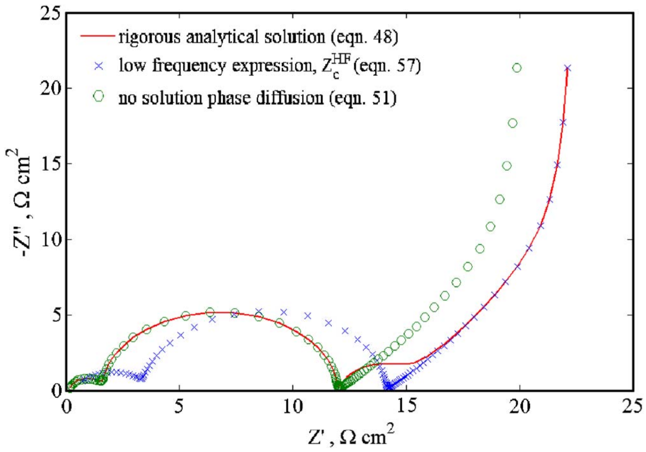

Figure 6. (Color online) Complex plane impedance plot showing the comparison of impedance of the insertion electrode, Z_c using the low frequency expression (Eq. 58) and high frequency expression (Eq. 57) against the rigorous analytical solution (Eq. 47). The terms Z' and Z'' denote the real and the imaginary part of the impedance respectively. The impedance values were obtained at 100 evenly spaced logarithmic frequency points between 10^5 Hz and 5×10^{-4} Hz at a state of charge, $\theta_c = 0.8$.

$$Z_c^{LF} = \frac{L_c}{\sigma_c^{eff}}\left[\gamma_1 + \frac{\gamma_2}{\sqrt{\Theta_1 + \Theta_2}\tanh\sqrt{\Theta_1 + \Theta_2}} + \frac{\gamma_3}{\sqrt{\Theta_1 + \Theta_2}\sinh\sqrt{\Theta_1 + \Theta_2}}\right] \qquad [57]$$

where γ_1, γ_2, and γ_3 are constants (real) and are not functions of frequencies (the values of γ_1, γ_2, and γ_3 are given in Appendix B). The above expression is derived based on the fact that the concentration in the solution-phase has reached a steady state at very low frequencies and the impedance is dominated by the insertion of the Li^+ in the active material particle (see Appendix B). Therefore Z_c^{LF} described in Eq. 57 will be valid in the frequency range after which the solution-phase diffusion has reached a pseudo-steady state and the impedance spectrum is dominated by solid-phase diffusion processes. Figure 6 shows the complex plane impedance plot comparing the low-frequency expression Z_c^{LF} with the rigorous analytical solution from Eq. 48. It is observed that at low frequencies Z_c^{LF} agrees well with the rigorous analytical solution. For comparison, the impedance spectrum obtained for a porous electrode in the absence of solution-phase diffusion (as given in Eq. 51), which is also valid in the high-frequency region, is plotted in Fig. 6. It can be seen that the impedance spectrum predicted by Eq. 51 agrees well with the rigorous solution at high frequencies but deviates at low frequencies. This is more clearly seen in the Bode plots (see Fig. 7) where the magnitude of the impedance predicted with Eq. 51 agrees with the rigorous solution at high frequencies and slowly deviates at $\sim$0.1 Hz and at lower frequencies, the low-frequency expression, Z_c^{LF} matches the rigorous solution. An important point worth noting here is that the expression Z_c^{LF} cannot capture the hump in the high-frequency Warburg region (Fig. 6) because Z_c^{LF} was evaluated by solving for the steady state diffusion equation. The hump occurs due to the transience in the solution-phase diffusion process and this transience is clearly observed in the Bode-phase angle plot for the rigorous solution, as shown in Fig. 7. Although Z_c^{LF} cannot capture the hump due to transience, it includes the effect of the solution-phase diffusion process within it. This can be illustrated using Fig. 6. For the impedance spectrum predicted using Z_c^{LF} in Fig. 6, the midfrequency arc extends until the solution-phase process has

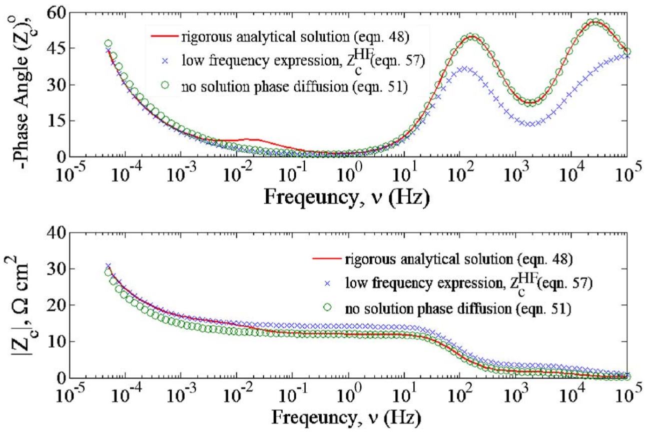

Figure 7. (Color online) Bode plots showing the phase difference and the magnitude of the impedance of the insertion electrode, Z_c using the low frequency expression (Eq. 58) and high frequency expression (Eq. 57) against the rigorous analytical solution (Eq. 47). The impedance values were obtained at 100 evenly spaced logarithmic frequency points between 10^5 Hz and 5×10^{-4} Hz at a state of charge, $\theta_c = 0.8$.

reached the steady state before the Warburg tail due to solid-phase diffusion starts. Thus, the expression for Z_c^{LF} can be used to estimate the diffusion coefficient in the insertion electrode more reliably than the traditional analytical expressions.

Determination of solid phase diffusion coefficient.— To evaluate the solid-phase diffusion coefficient by using the low-frequency intercept technique, the real part of the impedance expression extrapolated at zero frequencies should be evaluated and fit to experimentally measured low frequency resistance. Although the low-frequency expression Z_c^{LF} given by Eq. 57 is compact, analytical separation of real and imaginary parts is not straightforward. Thus, the expression is further simplified by assuming that at low frequencies, the charge-transfer resistance and the film resistance shorts the double-layer capacitance and the film capacitance, respectively, and β can be represented as

$$\left.\frac{1}{F\beta}\right|_{\omega\to 0} = \left[R_{ct} + R_{\text{film}} + \frac{1}{5}R_{\text{dif}} - j\frac{3}{\omega R_s F}\left(-\frac{dU}{dc_s}\right)\right] \qquad [58]$$

and as a result expression 57 reduces to (see Appendix C for derivation)

$$Z_{c,\omega\to 0}^{LF} = \frac{L_c}{\sigma_c^{\text{eff}}}\left[\gamma_1 + \frac{\gamma_2}{3} - \frac{\gamma_3}{6} + \frac{\gamma_2+\gamma_3}{\gamma_4 F\beta}\right] \qquad [59]$$

from which the real and imaginary components of the impedance are obtained as

$$\text{Re}[Z_{c,\omega\to 0}^{LF}] = \frac{L_c}{\sigma_c^{\text{eff}}}\left[\gamma_1 + \frac{\gamma_2}{3} - \frac{\gamma_3}{6} + \frac{\gamma_2+\gamma_3}{\gamma_4}\left(R_{ct} + R_{\text{film}} + \frac{1}{5}R_{\text{dif}}\right)\right]$$

$$\text{Im}[Z_{c,\omega\to 0}^{LF}] = \frac{L_c}{\sigma_c^{\text{eff}}}\left\{\frac{\gamma_2+\gamma_3}{\gamma_4}\left[-j\frac{3}{\omega R_s F}\left(-\frac{dU}{dc_s}\right)\right]\right\} \qquad [60]$$

Here, γ_1, γ_2, γ_3, and γ_4 are real constants and are not dependent on the value of the solid-phase diffusion coefficient, but include the effects due to solution-phase diffusion limitations. Hence, for the estimation of solid-phase diffusion coefficient, the real part of expression 59 as given in Eq. 60 should be used. When $\text{Re}[Z_{c,\omega\to 0}^{LF}]$ in Eq. 60 is turned around, the expression for the diffusion coefficient is obtained as

$$D_{\theta,c} = \frac{-\dfrac{1}{5}\dfrac{R_p}{F}\dfrac{\partial U}{\partial c_{\theta,c}}\dfrac{\gamma_2+\gamma_3}{\gamma_4}}{\dfrac{\sigma_c^{\text{eff}}}{L_c}\text{Re}[Z_{c,\omega\to 0}^{LF}] - \gamma_1 - \dfrac{\gamma_2}{3} + \dfrac{\gamma_3}{6} - \dfrac{\gamma_2+\gamma_3}{\gamma_4}(R_{ct} + R_{\text{film}})} \qquad [61]$$

This expression can be used to estimate the solid-phase diffusion coefficient of the active species by fitting the experimental data obtained on porous electrodes even in the presence of solution-phase diffusion limitations, provided the constant real part in the low-frequency impedance spectrum, $\text{Re}[Z_{c,\omega\to 0}^{LF}]$ is known. The expression captures the effect of the porous nature of the electrodes as well as the effect of solution-phase diffusion limitations in addition to the kinetic and solid-phase resistances. Figure 8 shows the comparison of solid-phase diffusion coefficient extracted from expression 61 and the traditional low frequency intercept given by[13,26]

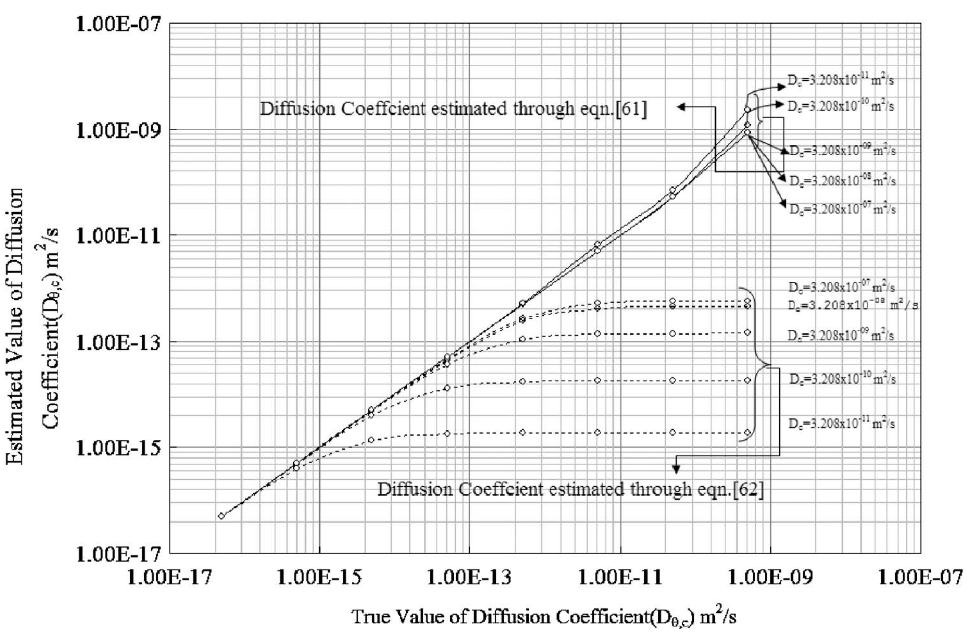

Figure 8. (Color online) Comparison of the estimation of solid phase diffusion coefficient from the low frequency intercept on the real axis using the standard formula (Eq. 61) represented by dashed lines and the new expression (Eq. 60) represented by solid lines. The low frequency resistance used for $\text{Re}[Z_{c,\omega\to 0}^{LF}]$ in either expression, is obtained by calculating the real part of the impedance at 10^{-6} Hz using Eq. 47. All values were calculated at a state of charge, $\theta_c = 0.8$. The values of the solution phase diffusion coefficient used for these calculations are marked against each curve.

$$D_{\theta,c} = \frac{R_p}{5Fa_cL_c \operatorname{Re}[Z^{LF}_{c,\omega\to 0}]}\left(-\frac{\partial U}{\partial c_{\theta,c}}\right) \quad [62]$$

Equation 62 is obtained by solving for the diffusion equation in a single spherical particle and scaling it to the total volumetric area of the electrode. The values for all the other parameters are the same and are listed in Table I. The value for $-\partial U_c/\partial c_\theta = -2.54 \times 10^{-6}$ (Vm^3/mol) is evaluated for the state of charge, $\theta_c = 0.8$. The true values of the diffusion coefficient (in the abscissa) are the values used to generate the synthetic impedance data from Eq. 48. The value for $Z^{LF}_{c,\omega\to 0}$ to be used to evaluate the diffusion coefficient using Eq. 61 and 62 is obtained from the low-frequency resistance calculated from the synthetic impedance data. It can be inferred from Fig. 8 that, the traditional expression 62 fails to predict the true value of the solid-phase diffusion coefficient, when the value of the solution-phase diffusion coefficient is low and/or when the value of the solution-phase diffusion coefficient is not well separated (by at least five or six orders of magnitude) from the solid-phase diffusion coefficient. For instance, when the value of solution-phase diffusion coefficient D_c is 3.208×10^{-10} m^2/s and the true value of the solid-phase diffusion coefficient is $D_{\theta,c} = 5 \times 10^{-13}$ m^2/s, the value of the solid-phase diffusion coefficient estimated using expression 62 is $D_{\theta,c} = 1.7362 \times 10^{-14}$ m^2/s, while the value estimated using expression 61 is $D_{\theta,c} = 5.00293 \times 10^{-13}$ m^2/s. Expression 62 underestimates the value of solid-phase diffusion coefficient for the above case by more than an order of magnitude. This is evident as expression 62 does not account for the solution-phase diffusion process, which is significant when the value of D_c gets closer to $D_{\theta,c}$. It should be noted that while estimating the diffusion coefficient using Eq. 62, a constant value of 11.85 Ω cm^2 (intercept of the impedance spectrum on the real axis in Fig. 2 for $\theta_c = 0.8$ in the midfrequency region) is subtracted from the true value of $\operatorname{Re}[Z^{LF}_{c,\omega\to 0}]$ to account for the charge transfer and the Ohmic resistance contribution, which is ignored in expression 62.

Although the expression for the low-frequency region given by Z^{LF}_c can be used in the transition region, it would not be always valid in the semi-infinite region of the Warburg region, because of the omission of the solution-phase diffusion transience in the expression, which could be significant when the values of solid- and solution-phase diffusion coefficients are comparable. This is also clearly seen in Fig. 6, where the low-frequency expression does not agree with the rigorous solution at the start of the Warburg region. Thus, the estimation of diffusion coefficient using the low-frequency expression Z^{LF}_c should be more accurate from the transition region and the low-frequency resistance, $Z^{LF}_{c,\omega\to 0}$, rather from the semi-infinite region. In the semi-infinite region of the Warburg impedance, the transience in the solution-phase diffusion process is predominant, and hence, expression 57 would not be appropriate, instead the rigorous analytical solution (Eq. 48) should be used to evaluate the diffusion coefficient.

Conclusions

An analytical expression for the impedance response of an insertion electrode in a cell is presented in this work. The analytical expression can be used to predict the impedance response of systems influenced by Ohmic, capacitive, and solid- and solution-phase diffusion limitations. An accurate expression to calculate the solid-phase diffusion coefficient in porous electrodes from the low-frequency resistance is also presented (Eq. 61). The analytical solution for the impedance response of a cell with an insertion electrode, separator, and a foil is also presented and can be used to simulate the impedance response for half cells and primary batteries. The analytical solution technique can also be extended to cells with dual insertion electrodes.

Acknowledgments

Financial support provided by National Reconnaissance Office (NRO) under contract no. NRO-000-03-C-0122 is gratefully acknowledged.

The University of South Carolina assisted in meeting the publication costs of this article.

Appendix A

Expression for the Impedance of the Insertion Electrode in the Absence of Solution-Phase Diffusion Limitations

In the absence of solution-phase diffusion limitations, the dimensionless parameter $\Theta_1 \simeq 1$, and since the diffusional resistance is also negligible compared to Ohmic resistance, $\Theta_1 \simeq \Theta_2$. As a result the eigenvalues, λ_1 and λ_2 reduce to

$$\lambda_1 = \frac{1}{2}\left[\bar{s}_c + \Theta_1 + \Theta_2 + \sqrt{\bar{s}_c^2 + 2\bar{s}_c(\Theta_1 - \Theta_2) + (\Theta_1 + \Theta_2)^2}\right] \simeq \bar{s}_c$$

$$\lambda_2 = \frac{1}{2}\left[\bar{s}_c + \Theta_1 + \Theta_2 - \sqrt{\bar{s}_c^2 + 2\bar{s}_c(\Theta_1 - \Theta_2) + (\Theta_1 + \Theta_2)^2}\right] \simeq \Theta_2 \quad [A-1]$$

Consequently, the expression for the impedance of cathode given by Eq. 48 reduces to

$$Z_c = \frac{L_c}{\sigma_c^{eff} + \kappa_c^{eff}} + \frac{L_c^3 a_c F\beta}{\sigma_c^{eff2}\Theta_1}\left\{\frac{\bar{s}_c - \Theta_2}{\Theta_2}\left(\frac{\Theta_1}{\sqrt{\Theta_2}(\bar{s}_c - \Theta_2)\tanh\sqrt{\Theta_2}} - \frac{C_4}{\sinh\sqrt{\Theta_2}}\right) + \frac{\bar{s}_c - \Theta_2}{\Theta_2}C_3\left(\frac{\sigma_c^{eff}\Theta_2}{L_c^2 a_c F\beta} - 1\right)\right\} \quad [A-2]$$

The value of the constants C_3 and C_4 from the expression 24 reduce to

$$C_3 = \frac{\Theta_1}{\sqrt{\Theta_2}(\bar{s}_c - \Theta_2)\sinh\sqrt{\Theta_2}} - \frac{C_4}{\tanh\sqrt{\Theta_2}}, \quad C_4 = -\frac{\sigma_c^{eff}\Theta_1}{\kappa_c^{eff}\sqrt{\Theta_2}(\bar{s}_c - \Theta_2)} \quad [A-3]$$

Plugging in the values of the constants in Eq. A-3 into the impedance expression A-2 yields

$$Z_c = \frac{L_c}{\sigma_c^{eff} + \kappa_c^{eff}} + \frac{L_c^3 a_c F\beta}{\sigma_c^{eff2}\Theta_1}\frac{\bar{s}_c - \Theta_2}{\Theta_2}\frac{\Theta_1}{\sqrt{\Theta_2}(\bar{s}_c - \Theta_2)}\left\{\left(\frac{1}{\tanh\sqrt{\Theta_2}} + \frac{\sigma_c^{eff}}{\kappa_c^{eff}}\frac{1}{\sinh\sqrt{\Theta_2}}\right) + \left(\frac{1}{\sinh\sqrt{\Theta_2}} + \frac{\sigma_c^{eff}}{\kappa_c^{eff}}\frac{1}{\tanh\sqrt{\Theta_2}}\right)\left(\frac{\sigma_c^{eff}\Theta_2}{L_c^2 a_c F\beta} - 1\right)\right\} \quad [A-4]$$

Using $\Theta_2 = L_c^2 a_c F\beta/\sigma_c^{eff}(1 + \sigma_c^{eff}/\kappa_c^{eff})$, the above expression can be further simplified to

$$Z_c = \frac{L_c}{\sigma_c^{eff} + \kappa_c^{eff}} + \frac{L_c}{\sigma_c^{eff} + \kappa_c^{eff}}\frac{\kappa_c^{eff}}{\sigma_c^{eff}}\frac{1}{\sqrt{\Theta_2}}\left\{\left(\frac{1}{\tanh\sqrt{\Theta_2}} + \frac{\sigma_c^{eff}}{\kappa_c^{eff}}\frac{1}{\sinh\sqrt{\Theta_2}}\right) + \left[\frac{\sigma_c^{eff}}{\kappa_c^{eff}}\frac{1}{\sinh\sqrt{\Theta_2}} + \left(\frac{\sigma_c^{eff}}{\kappa_c^{eff}}\right)^2\frac{1}{\tanh\sqrt{\Theta_2}}\right]\right\} \quad [A-5]$$

which can be grouped as

$$Z_c = \frac{L_c}{\sigma_c^{eff} + \kappa_c^{eff}}\left\{1 + \frac{1}{\sqrt{\Theta_2}}\left[\left(\frac{\kappa_c^{eff}}{\sigma_c^{eff}} + \frac{\sigma_c^{eff}}{\kappa_c^{eff}}\right)\frac{1}{\tanh\sqrt{\Theta_2}} + \frac{2}{\sinh\sqrt{\Theta_2}}\right]\right\} \quad [A-6]$$

This expression is similar to the solution for a porous electrode with linear kinetics as discussed by Newman.[31] It is worth nothing that the term $\sqrt{\Theta_2}$ has the variable β, which is a lumped parameter controlling the interfacial impedance as described by Eq. 15. The impedance of a porous electrode when β is purely Faradaic is discussed by Ong et al.[28] and a more complicated β for an interfacial model including particle size distribution is discussed by Meyers et al.[14] Analytical solutions are also available in the literature for the impedance of a porous electrode when β is purely capacitive[32,33] and pseudocapacitive.[34]

Appendix B

Expression for the Impedance of the Insertion Electrode in the Low-Frequency Region

In the low-frequency region a simplified expression for the impedance can be obtained by replacing Eq. 2 and 25 with the steady-state governing equations. This is justified by the fact that at very low frequencies when the impedance is dominated by insertion processes, the concentration in the solution phase reaches a steady state and neglecting for concentration variations will yield much simpler expression at low-frequency regions without compromising accuracy. Thus, at steady-state, Eq. 18 and 19 can be written as

$$\frac{d^2\tilde{\bar{c}}_c}{d\bar{x}_c^2} = -\Theta_1\tilde{\bar{\eta}}_c \quad [B-1]$$

$$\frac{d^2\tilde{\tilde{\eta}}_c}{d\bar{x}_c^2} = (\Theta_1 + \Theta_2)\tilde{\tilde{\eta}}_c \quad \text{[B-2]}$$

with the boundary conditions being the same as given in Eq. 20. In this case, Eq. B-1 and B-2 are not coupled and to evaluate the impedance it would be sufficient to solve for equation B-2 alone, with the boundary conditions

$$\bar{x}_c = 0: \quad \frac{d\tilde{\tilde{\eta}}_c}{d\bar{x}_c} - \frac{\Theta_1}{\Theta_2}\frac{F\left(1 + \frac{\sigma_c^{\text{eff}}}{\kappa_c^{\text{eff}}}\right)}{i_{\text{app}}(1 - t_+^0)}\xi^*(\bar{s}_c) = -\left(\frac{\sigma_c^{\text{eff}}}{\kappa_c^{\text{eff}}}\right)$$

$$\bar{x}_c = 1: \quad \frac{d\tilde{\tilde{\eta}}_c}{d\bar{x}_c} = 1 \quad \text{[B-3]}$$

Here, too, $\xi^*(\bar{s}_c)$ is an unknown constant that has to be determined by solving for the equations in the separator with the anode boundary. However, in this case $\xi^*(\bar{s}_c)$ reduces to a simple expression while solving for the concentration profiles in the separator. In the separator region Eq. 29 changes to

$$\frac{d^2\tilde{\tilde{c}}_s}{d\bar{x}_s^2} = 0 \quad \text{[B-4]}$$

with the boundary conditions from Eq. 31 written as

$$\bar{x}_s = 0, \quad \frac{d\tilde{\tilde{c}}_s}{d\bar{x}_s} = -\frac{L_s i_{\text{app}}}{c_B^0 F D_s^{\text{eff}}}(1 - t_+^0), \quad \bar{x}_s = 1, \quad \frac{d\tilde{\tilde{c}}_s}{d\bar{x}_s} = \frac{L_s}{c_B^0 D_s^{\text{eff}}}\xi^*(\bar{s}_s) \quad \text{[B-5]}$$

The solution for Eq. B-4 yields $d\tilde{\tilde{c}}_s/d\bar{x}_s$ to be a constant, and hence,

$$\left.\frac{d\tilde{\tilde{c}}_s}{d\bar{x}_s}\right|_{\bar{x}_s=0} = \left.\frac{d\tilde{\tilde{c}}_s}{d\bar{x}_s}\right|_{\bar{x}_s=1} \quad \text{[B-6]}$$

which yields

$$\xi^*(\bar{s}_s) = -\frac{i_{\text{app}}}{F}(1 - t_+^0) \quad \text{[B-7]}$$

Thus, solving Eq. B-2 with the boundary conditions as in Eq. B-3, we obtain

$$\tilde{\tilde{\eta}}_c = \frac{\cosh(\sqrt{\Theta_1 + \Theta_2}\bar{x}_c) + \left[\frac{\Theta_1}{\Theta_2} + \frac{\sigma_c^{\text{eff}}}{\kappa_c^{\text{eff}}}\left(1 + \frac{\Theta_1}{\Theta_2}\right)\right]\cosh(\sqrt{\Theta_1 + \Theta_2}(\bar{x}_c - 1))}{\sqrt{\Theta_1 + \Theta_2}\,\sinh(\sqrt{\Theta_1 + \Theta_2})} \quad \text{[B-8]}$$

The evaluation of the impedance of the cell from $\tilde{\tilde{\eta}}_c$ is done using the same procedure as in the text using Eq. 45 with the boundary conditions in Eq. 46. The resulting expression for $\tilde{\phi}_{1,c}$ is plugged into the expression for the cathode impedance (Eq. 43) to yield the impedance of the insertion electrode. The expression obtained after simplification can be written as

$$Z_c^{\text{LF}} = \frac{L_c}{\sigma_c^{\text{eff}}}\left[\gamma_1 + \frac{\gamma_2}{\sqrt{\Theta_1 + \Theta_2}\tanh\sqrt{\Theta_1 + \Theta_2}} + \frac{\gamma_3}{\sqrt{\Theta_1 + \Theta_2}\sinh\sqrt{\Theta_1 + \Theta_2}}\right] \quad \text{[B-9]}$$

where γ_1, γ_2, and γ_3 are constants (real) and are not functions of frequencies. The values for these constants are given as

$$\gamma_1 = 1 - \frac{\Theta_2}{\Theta_1 + \Theta_2}\left[\frac{\kappa_c^{\text{eff}}}{\sigma_c^{\text{eff}} + \kappa_c^{\text{eff}}}\right]$$

$$\gamma_2 = \frac{\sigma_c^{\text{eff}}}{\kappa_c^{\text{eff}}} + \left[1 + \frac{\sigma_c^{\text{eff}}}{\kappa_c^{\text{eff}}}\right]\frac{\Theta_1}{\Theta_2} - \frac{\Theta_1}{\Theta_1 + \Theta_2} - \frac{\Theta_2}{\Theta_1 + \Theta_2}\left[\frac{\sigma_c^{\text{eff}} - \kappa_c^{\text{eff}}}{\sigma_c^{\text{eff}} + \kappa_c^{\text{eff}}}\right]$$

$$\gamma_3 = 1 + \frac{\Theta_1}{\Theta_1 + \Theta_2} + \frac{\Theta_2}{\Theta_1 + \Theta_2}\left[\frac{\sigma_c^{\text{eff}} - \kappa_c^{\text{eff}}}{\sigma_c^{\text{eff}} + \kappa_c^{\text{eff}}}\right] \quad \text{[B-10]}$$

Appendix C

Series Approximation for the Impedance of the Insertion Electrode at Very Low Frequencies

At low frequencies the impedance expression can be written as (Eq. 57)

$$Z_c^{\text{LF}} = \frac{L_c}{\sigma_c^{\text{eff}}}\left[\gamma_1 + \frac{\gamma_2}{\sqrt{\Theta_1 + \Theta_2}\tanh\sqrt{\Theta_1 + \Theta_2}} + \frac{\gamma_3}{\sqrt{\Theta_1 + \Theta_2}\sinh\sqrt{\Theta_1 + \Theta_2}}\right] \quad \text{[C-1]}$$

From the expressions of Θ_1 and Θ_2, we can write

$$\frac{\Theta_1 + \Theta_2}{F\beta} = \frac{2RT(1 - t_+^0)^2 a_c L_c^2}{\bar{\upsilon}^+ F^2 D_c^{\text{eff}}}\left(\frac{1}{c_B^0} + \frac{f'_{\pm,c_B^0}}{f_{\pm,c_B^0}}\right) + L_c^2 a_c\left(\frac{1}{\sigma_c^{\text{eff}}} + \frac{1}{\kappa_c^{\text{eff}}}\right) = \gamma_4 \quad \text{[C-2]}$$

where γ_4 is a real quantity. Plugging Eq. C-2 into Eq. C-1

$$Z_c^{\text{LF}} = \frac{L_c}{\sigma_c^{\text{eff}}}\left[\gamma_1 + \frac{\gamma_2}{\sqrt{\gamma_4 F\beta}\tanh\sqrt{\gamma_4 F\beta}} + \frac{\gamma_3}{\sqrt{\gamma_4 F\beta}\sinh\sqrt{\gamma_4 F\beta}}\right] \quad \text{[C-3]}$$

At very low frequencies when $\omega \to 0$, from Eq. 58

$$(F\beta)|_{\omega\to 0} = \frac{1}{R_{\text{ct}} + R_{\text{film}} + \frac{1}{5}R_{\text{dif}} - j\frac{3}{\omega R_s F}\left(-\frac{dU}{dc_s}\right)} \simeq 0 \quad \text{[C-4]}$$

For very small values of β, taking the first two terms of the series expansion,

$$\frac{\gamma_2}{\sqrt{\gamma_4 F\beta}\tanh\sqrt{\gamma_4 F\beta}} = \frac{\gamma_2}{\gamma_4 F\beta} + \frac{\gamma_2}{3} \quad \text{[C-5]}$$

$$\frac{\gamma_3}{\sqrt{\gamma_4 F\beta}\sinh\sqrt{\gamma_4 F\beta}} = \frac{\gamma_3}{\gamma_4 F\beta} - \frac{\gamma_3}{6} \quad \text{[C-6]}$$

Thereby Eq. C-3 reduces to

$$Z_{c,\omega\to 0}^{\text{LF}} = \frac{L_c}{\sigma_c^{\text{eff}}}\left[\gamma_1 + \frac{\gamma_2 + \gamma_3}{\sqrt{\gamma_4 F\beta}} + \frac{\gamma_2}{3} - \frac{\gamma_3}{6}\right] \quad \text{[C-7]}$$

Appendix D

Expressions Used in LiCo O_2 Insertion Electrode

The active particles in the insertion electrode are assumed to be spherical and hence the active surface area to volume ratio is given by the relation

$$a_c = 3\left(\frac{1 - \varepsilon_c - \varepsilon_c^f}{R_c}\right) \quad \text{[D-1]}$$

The effective diffusion coefficient of Li^+ in the solution phase is given by the Bruggeman relation

$$D_c^{\text{eff}} = D_c \varepsilon_c^{\text{brug}_c} \quad \text{[D-2]}$$

Similarly, the effective conductivities of Li^+ in the solid phase and the solution phase are also related by the Bruggeman coefficient:

$$\sigma_c^{\text{eff}} = \sigma_c(1 - \varepsilon_c - \varepsilon_c^f)^{\text{brug}_c} \quad \text{[D-3]}$$

$$\kappa_c^{\text{eff}} = \kappa_c \varepsilon_c^{\text{brug}_c} \quad \text{[D-4]}$$

The activity coefficient as a function of salt concentration is given by[35]

$$\ln f_\pm = \frac{1}{1 - t_+^0}[-0.48\sqrt{c_c} + 0.67 c_c^{3/2}(2.4679 - 0.0051T)] \quad \text{[D-5]}$$

evaluated at 298 K and the concentration c_c is expressed in mol/dm^3

Electrode thermodynamic data for the open-circuit potential of $LiCoO_2$ electrode.— The open-circuit potential of the positive intercalation electrode ($LiCoO_2$) obtained from the Mine Safety Appliances Company (Sparks, MD) was fit to the function

$$U_c = \left\{\frac{4.0396 - 32.5724\left(\frac{c_s}{c_T}\right) + 104.8654\left(\frac{c_s}{c_T}\right)^2 - 168.3891\left(\frac{c_s}{c_T}\right)^3 + 134.6638\left(\frac{c_s}{c_T}\right)^4 - 42.6072\left(\frac{c_s}{c_T}\right)^5}{1 - 8.0912\left(\frac{c_s}{c_T}\right) + 26.1404\left(\frac{c_s}{c_T}\right)^2 - 42.1196\left(\frac{c_s}{c_T}\right)^3 + 33.7932\left(\frac{c_s}{c_T}\right)^4 - 10.7226\left(\frac{c_s}{c_T}\right)^5}\right\} \quad \text{[D-6]}$$

List of Symbols

- a specific surface area of the porous material, m^2/m^3
- c solution phase concentration, mol/m^3
- c_θ solid phase concentration, mol/m^3
- c_B^o initial bulk concentration in the solution phase, mol/m^3
- C_{dl} double layer capacitance, F/m^2
- C_{film} capacitance of the film, F/m^2
- D_θ diffusion coefficient of Li^+ in the solid phase, m^2/s
- D diffusion coefficient of the salt in the electrolyte, m^2/s
- $f_\pm$ activity coefficient of Li^+ in the electrolyte

$f'_{\pm}$ derivative of $f_{\pm}$ w r to c, m^3/mol
F Faraday's constant, 96487 C/eq.
i_0 exchange current density, A/m^2
i_1 solid phase current density, A/m^2
i_2 solution phase current density, A/m^2
i_{app} applied current density, A
i_F Faradaic current density, A/m^2
i_{dl} double layer current density, A/m^2
i_n total outward normal current density, A/m^2
L_c thickness of the cathode, m
L_s thickness of the separator, m
n number of electrons transferred in the intercalation reaction, $n = 1$
j_n reaction rate at the pore wall interface, mol/m^2/s
r radial coordinate within an active material particle, m
R ideal gas constant, 8.3143 J/mol/K
R_{ct} charge transfer resistance defined as $RT/i_{0,c}(\alpha_{a,c} + \alpha_{c,c})F$, Ω m^2
R_{dif} solid phase diffusional impedance, $-(R_p/D_{\theta,c}F)(\partial U/\partial c_{\theta,c})$, Ω m^2
R_{film} resistance of the surface film, Ω m^2
R_p radius of solid spherical particles, m
s Laplace variable, $j\omega$
$\bar{s}_c$ dimensionless Laplace variable in the intercalation electrode $(\varepsilon_c L_c^2 s/D_c^{eff})$, s^{-1}
$\bar{s}_s$ dimensionless Laplace variable in the separator region given by $(\varepsilon_s L_s^2 s/D_s^{eff})$, s^{-1}
$\bar{s}_a$ dimensionless Laplace variable in the anode region given by s, s^{-1}
t_+^0 transference number of Li^+ in the electrolyte
t time, s
T temperature, K
U open circuit potential, V
V Eigen Vector, defined in Eq. 23
x spatial dimension (distance from the anode surface), m
Y_s transfer function as defined in Eq. 16
Z_{cell} total impedance of the electrochemical cell, Ω m^2

Greek

α transfer coefficient
ε porosity of composite electrode
η electrochemical reaction over potential $(\phi_1 - \phi_2)$, V
κ solution phase conductivity, S/m
σ solid phase conductivity, S/m
ϕ_1 solid phase potential, V
ϕ_2 solution phase potential, V
$\tilde{\phi}_1$ perturbed solid phase potential, V
$\tilde{\phi}_2$ perturbed solution phase potential, V
Θ_1 dimensionless parameter,

$$\frac{2RT(1-t_+^0)^2 a_c L_c^2}{\tilde{\upsilon}^+ F^2 D_c^{eff}}\left(\frac{1}{c_B^0} + \frac{f'_{\pm,c_B^0}}{f_{\pm,c_B^0}}\right) \Bigg/ \frac{1}{F\beta}$$

Θ_2 dimensionless parameter,

$$L_c^2 a_c\left(\frac{1}{\sigma_c^{eff}} + \frac{1}{\kappa_c^{eff}}\right) \Bigg/ \frac{1}{F\beta}$$

Θ_3 dimensionless parameter,

$$\frac{2RT(1-t_+^0)c_B^0}{F}\left(\frac{1}{c_B^0} + \frac{f'_{\pm,c_B^0}}{f_{\pm,c_B^0}}\right)$$

λ_1,λ_2 eigenvalues as defined in Eq. 22
ν frequency, Hz
ω frequency, $2\pi\nu$, s^{-1}
$\tilde{\upsilon}^+$ number of cations into which a mole of electrolyte dissociates
$\gamma_1,\gamma_2,\gamma_3$ constants defined in Eq. B-10
γ_4 $(\Theta_1 + \Theta_2)/F\beta$

Subscripts

c intercalation electrode, cathode
s separator
a foil anode
θ solid phase of the intercalation electrode

Superscripts

overbar dimensionless variables
~ variables in the Laplace domain
eff effective values
f filler

References

1. K. Dokko, M. Mohamedi, Y. Fujita, T. Itoh, M. Nishizawa, M. Umeda, and I. Uchida, *J. Electrochem. Soc.*, **148**, A422 (2001).
2. M. D. Levi, G. Salitra, B. Markovsky, H. Teller, D. Aurbach, U. Heider, and L. Heider, *J. Electrochem. Soc.*, **146**, 1279 (1999).
3. P. Yu, B. N. Popov, J. A. Ritter, and R. E. White, *J. Electrochem. Soc.*, **146**, 8 (1999).
4. M. G. S. R. Thomas, P. G. Bruce, and J. B. Goodenough, *J. Electrochem. Soc.*, **132**, 1521 (1985).
5. D. Zhang, B. S. Haran, A. Durairajan, R. E. White, Y. Podrazhansky, and B. N. Popov, *J. Power Sources*, **91**, 122 (2000).
6. J. Fan and P. S. Fedkiw, *J. Power Sources*, **72**, 165 (1998).
7. D. Aurbach, B. Markovsky, A. Rodkin, M. Cojocaru, E. Levi, and H. J. Kim, *Electrochim. Acta*, **47**, 1899 (2002).
8. M. Dolle, F. Orsini, A. S. Gozdz, and J. M. Tarascon, *J. Electrochem. Soc.*, **148**, A851 (2001).
9. R. Bouchet, S. Lascaud, and M. Rosso, *J. Electrochem. Soc.*, **150**, A1385 (2003).
10. M. S. Wu, P. C. J. Chiang, and J. C. Lin, *J. Electrochem. Soc.*, **152**, A47 (2005).
11. C. S. Wang, A. J. Appleby, and F. E. Little, *J. Electrochem. Soc.*, **150**, A143 (2003).
12. I. D. Raistrick, *Electrochim. Acta*, **35**, 1579 (1990).
13. M. Doyle, J. P. Meyers, and J. Newman, *J. Electrochem. Soc.*, **147**, 99 (2000).
14. J. P. Meyers, M. Doyle, R. M. Darling, and J. Newman, *J. Electrochem. Soc.*, **147**, 2930 (2000).
15. Q. Z. Guo, V. R. Subramanian, J. W. Weidner, and R. E. White, *J. Electrochem. Soc.*, **149**, A307 (2002).
16. S. Devan, V. R. Subramanian, and R. E. White, *J. Electrochem. Soc.*, **151**, A905 (2004).
17. P. M. Gomadam, J. W. Weidner, T. A. Zawodzinski, and A. P. Saab, *J. Electrochem. Soc.*, **150**, E371 (2003).
18. D. Dees, E. Gunen, D. Abraham, A. Jansen, and J. Prakash, *J. Electrochem. Soc.*, **152**, A1409 (2005).
19. J. Newman and C. W. Tobias, *J. Electrochem. Soc.*, **109**, 1183 (1962).
20. P. DeVidts and R. E. White, *J. Electrochem. Soc.*, **144**, 1343 (1997).
21. M. W. Verbrugge and B. J. Koch, *J. Electrochem. Soc.*, **150**, A374 (2003).
22. Q. Z. Guo and R. E. White, *J. Electrochem. Soc.*, **152**, A343 (2005).
23. S. Motupally, C. C. Streinz, and J. W. Weidner, *J. Electrochem. Soc.*, **142**, 1401 (1995).
24. G. Sikha, B. N. Popov, and R. E. White, *J. Electrochem. Soc.*, **151**, A1104 (2004).
25. E. Kreyszig, *Advanced Engineering Mathematics*, 7th ed., John Wiley & Sons, New York, p. 159 (1993).
26. T. Jacobsen and K. West, *Electrochim. Acta*, **40**, 255 (1995).
27. A. Lasia, *J. Electroanal. Chem.*, **428**, 155 (1997).
28. I. J. Ong and J. Newman, *J. Electrochem. Soc.*, **146**, 4360 (1999).
29. C. Ho, I. D. Raistrick, and R. A. Huggins, *J. Electrochem. Soc.*, **127**, 343 (1980).
30. B. S. Haran, B. N. Popov, and R. E. White, *J. Power Sources*, **75**, 56 (1998).
31. J. Newman, *Electrochemical Systems*, 2nd ed., Prentice-Hall, Englewood Cliffs, NJ (1991).
32. A. M. Johnson and J. Newman, *J. Electrochem. Soc.*, **118**, 510 (1971).
33. V. Srinivasan and J. W. Weidner, *J. Electrochem. Soc.*, **146**, 1650 (1999).
34. V. R. Subramanian, S. Devan, and R. E. White, *J. Power Sources*, **135**, 361 (2004).
35. L. O. Valoen and J. N. Reimers, *J. Electrochem. Soc.*, **152**, A882 (2005).